Characterization of Mechanical Loading on Human Ribs During Ventilation

Undergraduate Research Thesis

Presented in Partial Fulfillment of the Requirements for

Graduation with Distinction

at The Ohio State University

By

Reagan Di Iorio

The Ohio State University

2020

Defense Committee:

Dr. Mandy Agnew, Advisor

Dr. Yun-Seok Kang

Dr. John Bolte, IV

Abstract

Bone is a complex adaptive system, remodeling to accommodate mechanical and metabolic stimuli. The mechanical drivers for functional adaptation have been well characterized in weight-bearing bones such as the tibia, where the shape and function are intuitively connected. To understand the unusual morphology of ribs, the loading environment of ribs during respiration can be recapitulated to determine the mechanical stimuli that drive functional adaptation, which can be used to better define increased fracture risk. One post-mortem human subject (PMHS) was instrumented with strain gages on the cutaneous and pleural surfaces of ribs 3-9 and the sternum. A bladder and air pump were used to recapitulate ventilation in a series of shallow and deep breaths. The study will focus on strain coupling between the pleural and cutaneous surfaces of individual ribs and the behaviors of ribs at different levels, especially concerning the upper level ribs connected directly to the sternum. Characterizing the internal loading environment of ribs during breathing will enable researchers to better understand and characterize risk of rib fracture from blunt force trauma. Furthermore, the increased understanding of the bone morphology will help determine the directions of robust fracture resistance versus in traumatic impacts and provide more accurate subject-specific input to finite element models.

Acknowledgements

I would like to thank my advisor, Dr. Mandy Agnew, for her continual support and patience throughout this process. I would also like to thank Dr. Yun-Seok Kang for his data analysis wizardry. A special thanks to both, for believing in me more than I did myself. Finally, I would like to thank all the students, staff, and faculty of the Injury Biomechanics Research Center (IBRC) at The Ohio State University for their support; moral, pinned, and otherwise, especially Akshara Sreedhar and Angela Harden.

Vita

NAME OF AUTHOR ..... Reagan Sean Di Iorio
DATE AND PLACE OF BIRTH ..... June 7, 1998, Rockford, IL
FIELD OF STUDY ..... Biomedical Engineering

Table of Contents

List of Figures

List of Tables

Introduction

Background and Motivation

Bone is a complex adaptive system, coordinating to adjust in response to mechanical and metabolic stimuli to establish and maintain systemic homeostasis [1-6]. Clinical interest lies primarily in homeostasis to preserve mechanical integrity, because some individuals experience increased fracture susceptibility despite adapting to environmental stimuli by similarly hypothesized mechanisms [7]. Such mechanical drivers for functional adaptation have been well characterized in weight-bearing bones such as the tibia [7], where the shape and function are intuitively connected.

Ribs are morphologically unique, and many of the simple-beam model or uniaxial loading simplifications typically applied to long bones cannot be utilized. While human ribs pose an unusual challenge, they also demonstrate relatively similar loading environments across populations, because the main forces on the ribs are due to respiration, which is important regardless of lifestyle. Despite the similarities in loading, ribs demonstrate enormous morphological variation. This leads to an associated variation in fracture risk and differences in biomechanics. To understand the morphology of ribs, the loading environment of ribs during respiration can be simulated to determine the mechanical stimuli that drive functional adaptation.

In studies to date, rib fractures and pathology have been characterized retrospectively. Chest wall disorders impair normal breathing without affecting the lungs themselves, decreasing total lung capacity and respiratory efficiency [8]. Pectus deformities affect approximately one in four hundred people, increasing in severity during adolescent growth years [9]. More commonly, scoliosis is associated with rib cage deformities that compromise cardiopulmonary function to

varying degrees [10]. Flail chest injuries, defined by fractures of 3 or more consecutive ribs fractures in 2 or more places, predispose to acute respiratory distress syndrome [11]. These various injuries to the ribs or pathologic deviations from typical ribcage construction change the ribcage biomechanics, and have profound impacts on breathing, independent of lung injury or abnormality.

While pathologic effects on the ribcage on breathing have been studied extensively, little is known regarding characteristic mechanical loading of ribs during normal breathing. The mechanical properties of individual ribs have been investigated through destructive testing [12]. As a result, the current understanding of mechanical loading on ribs is limited to research in areas of rib fracture and traumatic injury. Exploratory studies investigated changes in sternal angle with breathing [13] and rib cage distortion with exercise [14], but little is known about the internal mechanical loading of ribs during breathing.

Physiology of Ventilation

The act of breathing is driven by a gradient between the external atmospheric pressure and pressure in the lungs, in accordance with Boyle's Law, which states that in a gas, pressure increases as volume decreases. During inspiration, the diaphragm and external intercostal muscles are recruited to expand the thoracic cavity, leading to a decrease in intra-alveolar pressure. The decrease creates a pressure gradient that brings air into the lungs. Normal expiration is a passive process, as the elasticity of the lungs causes a recoil as the diaphragm and intercostal muscles relax, leading to a rise in interpulmonary pressure and thus causes air to leave the lungs.

Ventilation is further affected by the contraction and relaxation of the diaphragm and accessory musculature of the thorax. Additionally, the size of the airway affects the resistance of gas flow in and out of the lungs. Finally, thoracic wall compliance, or the ability of the thoracic wall to deform under pressure, affects ventilation and the effort that must be expended to facilitate ventilation.

Objective

The objective of this study was to characterize the loading environment of ribs during simulated ventilation. This was accomplished by analyzing strain data from various ribs and identifying pattern differences based on rib level, location on the rib, and bony surface. It was hypothesized that strain magnitude and strain mode would be similar for all rib levels, similar between locations on the same rib, and the cutaneous and pleural strains experienced at the same gage location would be opposite in mode but similar in magnitude.

Methods

Overview

Testing was conducted in four Phases and designed so that data could be compared between Phases to ensure the ventilation was consistent (Figure 1, Table 1). The first three Phases were performed to determine if strain patterns observed during *in vivo* ventilation could be effectively determined in a PMHS model, while Phase IV served to identify variation in the strain modes and magnitudes across the thorax during ventilation.

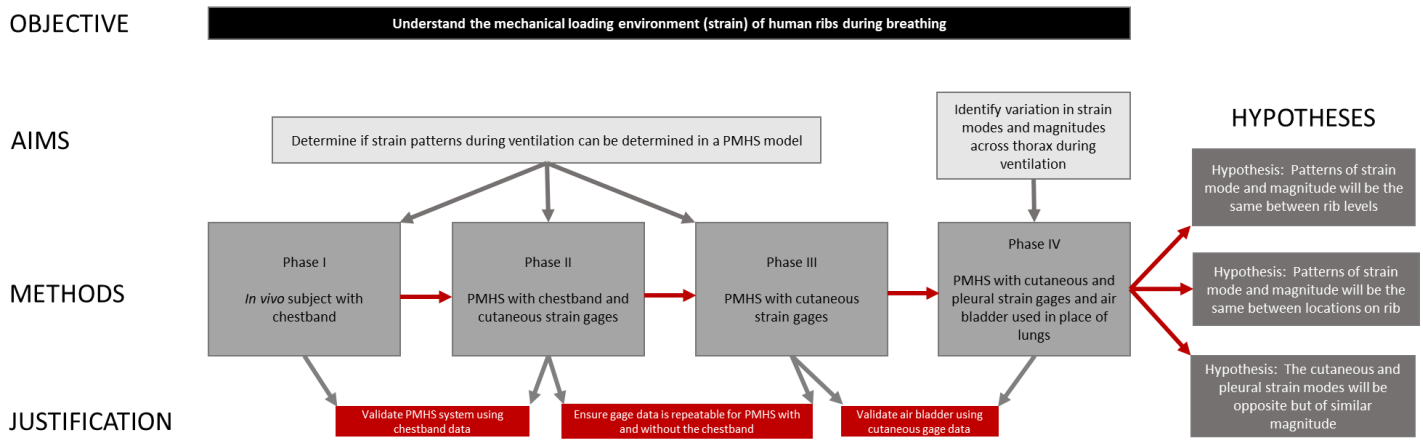

Figure 1. A flow chart with an overview of the objective, aims, experimental procedure, justification, and hypotheses.

Phase I began with a noninvasive measurement of strain using an external chestband on an *in vivo* volunteer, who was instructed on a sequence of breaths. In Phase II, the same chestband was used on a post-mortem human subject (PMHS), instrumented with additional strain gages on the cutaneous surface of the ribs. Ventilations were performed and the strain data from the chestband used in Phases I and II were compared to ensure the PMHS was behaving similarly to the *in vivo* volunteer. In Phase III, the chestband was removed from the PMHS and the procedure was repeated. The strain data from the cutaneous strain gages in Phases II and III were compared to determine whether the presence of the external chestband affected the loading environment of the ribs during breathing. Finally, the subject was further instrumented with pleural strain gages and the lungs were replaced with an air bladder in Phase IV. Ventilations were performed, and the cutaneous strain gage data from Phases III and IV were compared to determine whether the air bladder was a suitable substitute for the lungs.

Table 1. Test matrix. Phase I was performed with a volunteer subject, while the following Phases were conducted with a PMHS.

	Instrumentation			Ventilation	
Phase	Chestband	Cutaneous Gages	Pleural Gages	Lungs	Air Bladder
Phase I	■			■	
Phase II	■	■		■	
Phase III		■		■	
Phase IV		■	■		■

The cells filled in black indicate the instrumentation and ventilation specifications for each Phase of testing.

The cutaneous strain gage data from Phases II through IV and the pleural strain gage data from Phase IV were further analyzed to determine trends across the thorax, especially looking at variation between rib levels, at the same rib, and differences on the cutaneous and pleural cortices of the rib at the same location.

Phase I

A male volunteer was recruited for the *in vivo* Phase I testing. The subject was healthy and of approximately 50th percentile male anthropometry. The *in vivo* testing was conducted with a chestband, consisting of forty strain gages evenly spaced at one inch apart. The chestband was attached to the data acquisition system (DAS) and calibrated prior to obtaining data. The chestband was wrapped around the subject's thorax, centered at the sternum. To ensure flush contact with the skin, double sided tape was applied between the subject and underside of the chestband. The location of the chestband gages relative to the subject's sternum and spine were recorded.

The subject was instructed to complete a series of shallow and deep breath over sixty seconds of data collection. The data were collected in units of strain (rad/mm). The subject was first instructed to completely exhale and hold their breath for roughly ten seconds, then breathe normally for twenty seconds. The subject then breathed as deeply as possible for three consecutive breaths before breathing normally for the duration of the trial. The entire series of breaths was repeated four times, resulting in a total of 20 shallow breaths and 12 deep breaths.

Phase II

A male, fresh-frozen post-mortem human subject (PMHS) of approximately 50th percentile male anthropometry was used to conduct the PMHS tests in Phases II-IV of testing. The lungs and thorax were previously healthy, and the cause of death was unrelated to cardiopulmonary function. A dual-energy X-ray absorptiometry (DXA) scan for bone mineral density (BMD) confirmed the subject was not osteoporotic, with a lumbar T-score 1.9, and a computerized tomography (CT) scan verified the subject's thorax was intact and no decay was present. The PMHS was instrumented with strain gages (VISHAY Measurement Group, CEA-06-062UW-350, Raleigh, NC) bilaterally on the cutaneous surface of ribs 3-9 (Figure 2). A total of forty-two cutaneous strain gages were applied.

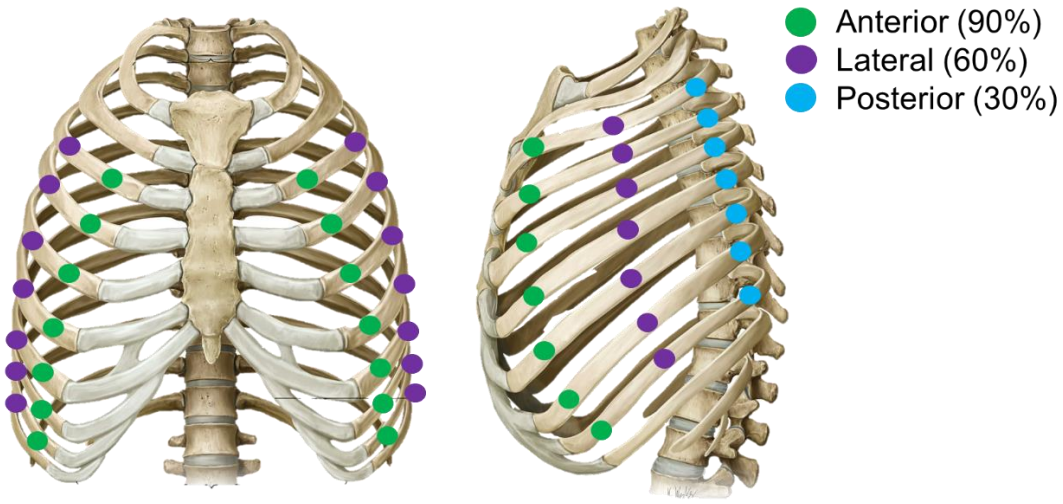

Figure 2. Placement of cutaneous strain gages on the PMHS thorax at anterior, lateral, and posterior sites.

The strain gages were placed at three positions: posterior, lateral, and anterior on the cutaneous cortex; 30%, 60%, and 90%, respectively, of the curve length of each rib (Figure 3), calculated from the CT scan.

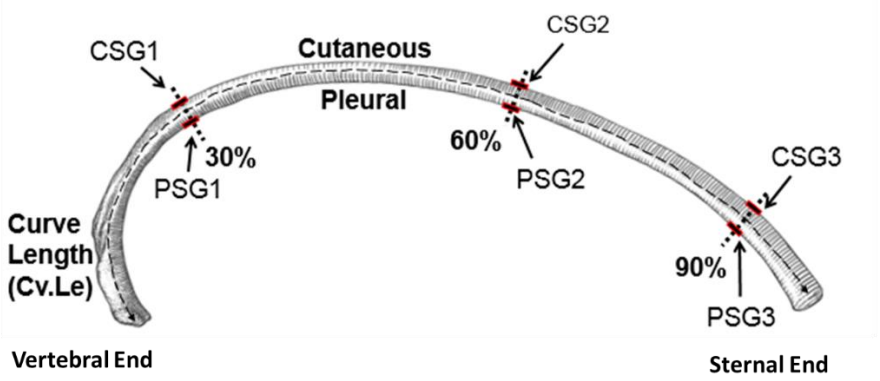

Figure 3. Strain gage placement on a single rib, with designations for the 30%, 60%, and 90% sites.

The strain gage placement was chosen in accordance with previous testing on structural properties of ribs [12].. The skin and soft tissue were reflected medially from the ribs, and the periosteum was carefully scraped off with a scalpel and cleaned with ether to prepare a small

space for strain gage placement. Gel super glue (Loctite) was added in thin layers over the cleaned bone to seal the dry, prepared surface and the strain gage was secured to the bone with more gel super glue. The gage was protected from potential moisture by two coats of acrylic paint (Figure 4).

Figure 4. On the left, a cutaneous strain gage with acrylic coating applied to the lateral site of L8, and on the right, an uncovered gage applied to the lateral site of L7.

After the acrylic dried, the strain gages were tested with a voltmeter to affirm the gages were functional and had not been compromised by moisture. The loose wires were secured to relieve strain exerted on the gages by the wires and prevent the gages from being removed from the bone. The steps were repeated for each strain gage.

The PMHS was secured in an upright sitting position and the hips and shoulders were aligned (Figure 5). In addition to the cutaneous strain gages, the same chestband used with the *in vivo* subject in Phase I was wrapped around the PMHS thorax and centered at the sternum. A tracheostomy was performed on the PMHS to access the lungs, and a resuscitation air bag was connected to a tracheal tube and used to inflate the PMHS lungs.

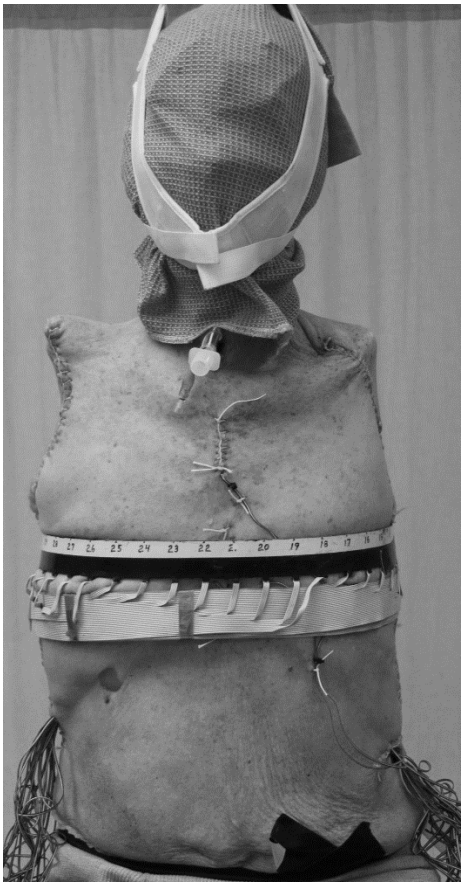

Figure 5. The PMHS seated upright in preparation for Phase II of testing.

The intrapulmonary pressure was increased until the PMHS chestband data matched the *in vivo* data from Phase I. The resuscitation air bag was manually inflated to replicate a series of shallow and deep breaths. Three trials were completed, and each lasted for sixty seconds, for a total of 10 shallow and 5 deep breaths.

Phase III

To mitigate any external loading or restriction of mobility resulting from the chestband, the chestband was removed from the PMHS. Instrumented with only the cutaneous strain gages, two trials were completed, each lasting sixty seconds, for a total of 11 shallow and 4 deep breaths.

Phase IV

The thoracic organs were eviscerated from the PMHS to attach strain gages to the pleural surfaces of ribs 4-8 and insert an air bladder as a surrogate for the lungs. The PMHS was placed in a supine position and an incision was made above the sternal notch, then another four inches superior. All vasculature, nerves, and muscles of the anterior neck were severed. The C7 and T1 vertebrae were separated to completely remove the head and neck. A transverse incision was made across the abdomen and the abdominal wall was separated from the ribs and reflected inferiorly. The greater omentum was pulled superiorly to access the intestines. The colon and associated vasculature were detached, and the esophagus was cut and sealed inferior to the diaphragm. The stomach, duodenum, and pancreas were detached, and the liver detached by severing the falciform and left triangular ligaments. The kidneys and urinary system were left intact. An incision was made through the diaphragm at the inferior margins of the ribs, and the trachea, esophagus, and connecting organs were pulled inferiorly. All remaining attachments were severed.

Strain gages were attached to the pleural cortex of the ribs using the same procedure utilized for the cutaneous strain gages.

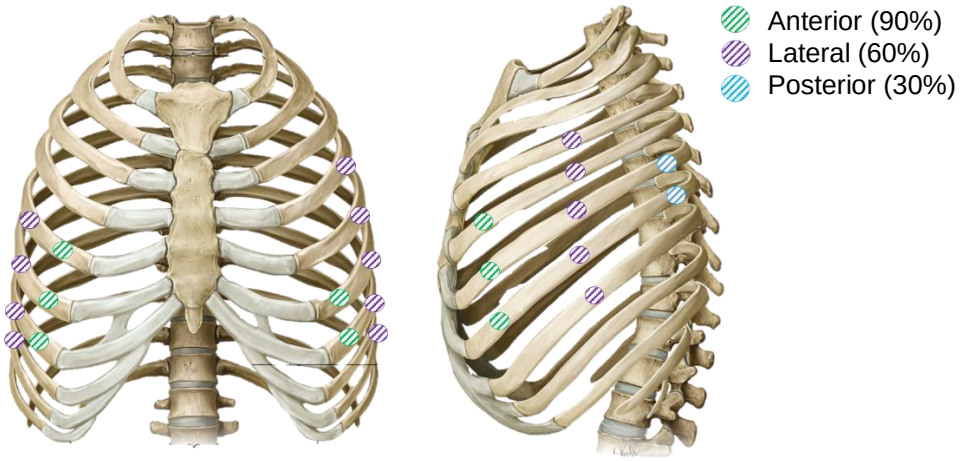

Figure 6. Placement of pleural strain gages on the PMHS thorax at anterior, lateral, and posterior sites.

The pleural side of the ribs was less accessible, even after eviscerating the thoracic organs, so fewer strain gages were applied at ribs four through eight, for a total of eighteen strain gages (Figure 6). As a result, most of the strain gages were placed at the lateral site (Figure 7).

Figure 7. A pleural strain gage applied to the lateral site of R7.

To act as a surrogate for the lungs, an air bladder was inserted in the thoracic cavity and inflated using a resuscitation pump (Figure 8).

Figure 8. The air bladder inserted as a surrogate for the lungs in Phase IV.

A Hybrid III 50th percentile ATD (Humanetics) abdomen was inserted to account for the spatial presence of the thoracic organs. The PMHS abdomen was sutured close.

The PMHS was once more placed in an upright, seated position with the hips and shoulders aligned. Due to the absence of lungs, the pressure required to inflate the air bladder to replicate mechanical loading in Phases I through III was unknown. Therefore, each trial was performed with a single ventilation to the maximum pressure of the air pump, approximately 120 cm H_2O, followed by a complete deflation of the air bladder. Each trial was sixty seconds in duration, and six trials were completed.

Data Processing

Data processing and analysis was performed in MATLAB (Mathworks). The polarity of all strain gage data were reversed in polarity to account for the strain gage boards used in data acquisition. All data, including both strain gage and chestband, were zeroed based on the first 120 milliseconds of data collection. A 4-pole, phaseless Butterworth filter with cutoff frequency 0.5 Hz was applied to all data to reduce noise while preserving trends (Figure 9).

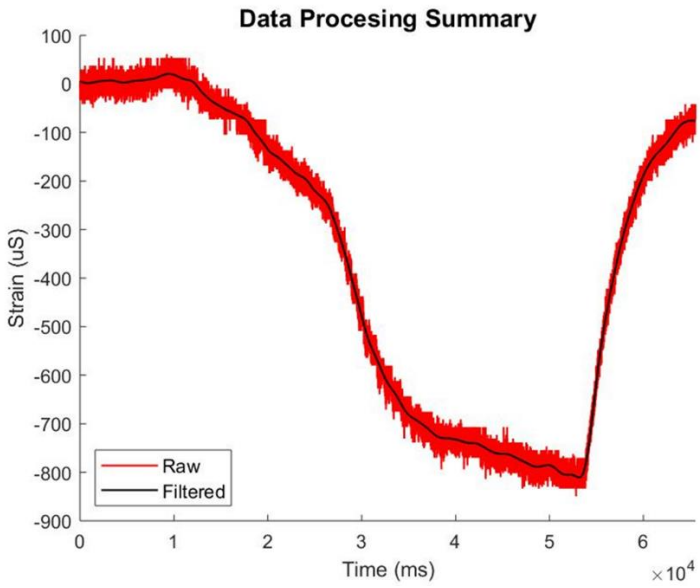

Figure 9. A time history plot from Phase IV with the raw data in red and the filtered data overlaid in black.

Results & Discussion

Validating the PMHS System

To ensure the ventilation observed in the *in vivo* subject was accurately represented in the PMHS system, strain gage data from the chestband data used in Phases I and II were compared. The chestband regions of interest were defined by relevant anatomical landmarks (Figure 10) based on the spine and sternum.

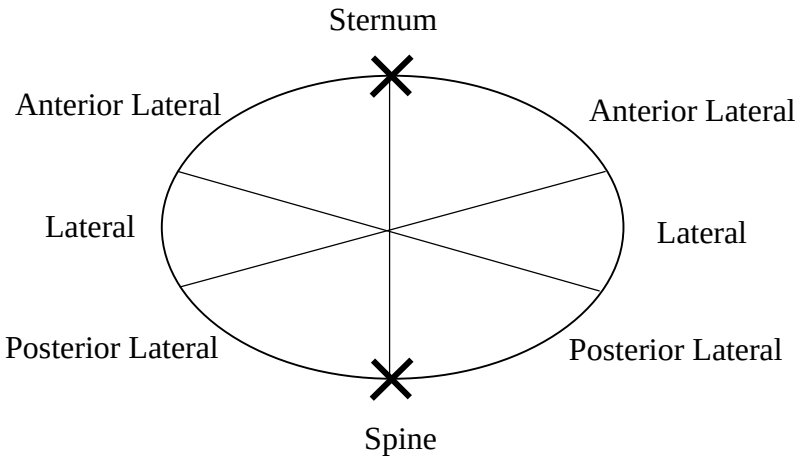

Figure 10. A map of the chestband regions of interest.

Gages from within each specified region were selected from both Phases I and II, because the slight variations in anthropometry between the *in vivo* volunteer and PMHS resulted in different gages at the same anatomical locations. For example, on the *in vivo* subject gages 21 and 22 were centered at the sternum, but for the PMHS, gages 22 and 23 were at the sternum (Table 2). Therefore, gages were selected for comparison based on their anatomical location and not the gage number. Time history plots of the selected gages were visually inspected to ensure there was not excessive noise or evidence of malfunction. Trials were omitted from gages with an asterisk (Table 2).

Table 2. Chestband Gages of interest.

	Sternum	Anterior Lateral (Left)	Anterior Lateral (Right)	Lateral (Left)	Lateral (Right)	Posterior Lateral (Left)	Posterior Lateral (Right)	Spine	Active Gages
in vivo	21,22	17,18	26,27	13,14	30,31	8,9	34,35	2,3	37
PMHS	22,23*	16*,17,18	25,27	13,14	29,30*	8,9	33,34	3*,4	36

**The asterisks denote a gage for which not all tests were used, i.e. PMHS 23* signifies trials 1 and 2 were omitted due to excessive noise.*

These included omitting trials 1 and 3 from PMHS gage 3, trial 1 from PMHS gage 16, trials 1 and 2 from PMHS gage 23, and omitting trials 1 and 2 from PMHS gage 30. The breath patterns documented in the procedure were used to segment each trial into shallow and deep breaths. The rise and fall of the chest were clearly visible in each time history plot (Figure 11), and the known breath patterns were used to inform the designation of relative peaks. For each breath, including the example in the gray box, the relative peak was quantified as the absolute value of the maximum strain minus the minimum strain over the time interval containing the breath (Figure 11).

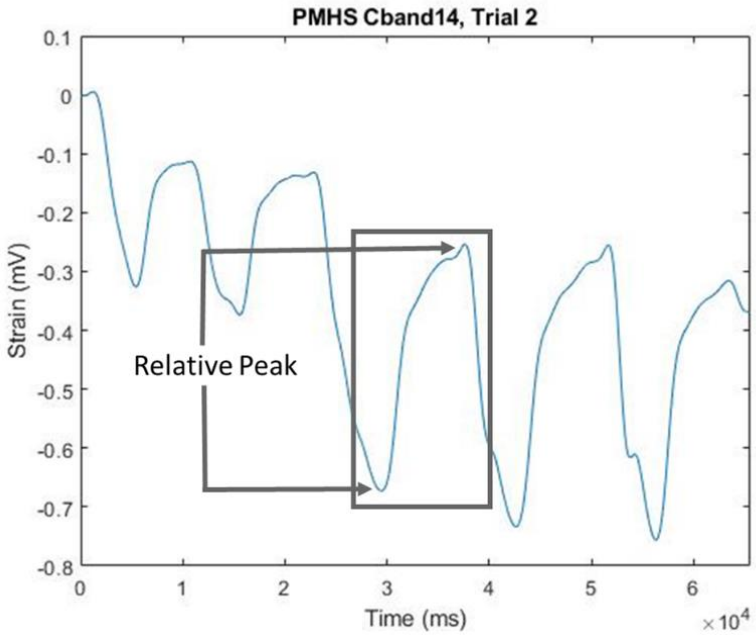

Figure 11. A visual representation of the relative peak measurement, which equates to maximum minus minimum strain for a single breath.

The negative strain magnitudes indicate the gage was in tension, and the peak strains were more negative than the momentary rest between breaths. The first two smaller breaths were shallow breaths, while the next was a deep breath. Even with the release of air between breaths, the momentary rest did not reach zero strain after the initial release. This was likely due to all air being expelled before the first few seconds of data collection, while for the remainder of the trial, there was some quantity of air in the lungs, similar to residual lung capacity, even when air was inspired and expired. This phenomenon contributed to the decision to use relative peak measurements, rather than an absolute peak, because the release of air after the first breath did not return completely to zero strain.

The data for Phase I were collected in rad/mm while the data for Phase II were collected in mV. To effectively compare their magnitude, the relative peaks from both data sets were normalized by conversion to a unitless M-score (Equation 1).

$$M - score = \frac{relative\ peak}{average\ relative\ peak\ from\ region\ of\ interest} \qquad \textit{Equation 1}$$

Statistics were computed in Minitab to compare Phase I and Phase II gages from the same region of interest on the Chestband. Each relative peak, corresponding to a single breath, was treated as a single observation. A Mann-Whitney test was performed with significance level 0.05 to compare the observations from Phases I and II (Table 3).

Table 3. Results of Mann-Whitney significance test between Phases I and II for both shallow and deep breaths.

Region of Interest	Sternum	Anterior Lateral (Left)	Anterior Lateral (Right)	Lateral (Left)	Lateral (Right)	Posterior Lateral (Left)	Posterior Lateral (Right)	Spine

p-value (shallow)	0.755	0.993	0.633	0.610	0.627	0.267	0.719	0.821
p-value (deep)	1.000	0.554	0.748	0.723	0.735	0.985	0.533	0.795

No significant difference was observed between the chestband strain data from Phases I and II, confirming there was no significant difference between the *in vivo* volunteer and PMHS ventilation ($p > 0.25$), thus validating the use of a PMHS system to replicate ventilation.

Validating Use of the Chestband

To ensure the presence of the chestband in Phases I and II did not significantly affect the strain experienced by the ribs, the cutaneous strain gage data from Phases II and III were compared. Because the chestband was wrapped completely around the *in vivo* subject and PMHS at sternum level, it was important to quantify any additional loading or restriction of movement that resulted from the presence of the chestband.

The breath patterns documented in the procedure were used to segment each trial into shallow and deep breaths. For each breath, the relative peak was once again quantified as the absolute value of the maximum strain minus the minimum strain over the time interval containing the breath (Figure 12). The gray box encapsulates a single shallow breath from Trial 2 of Phase III, shown in orange.

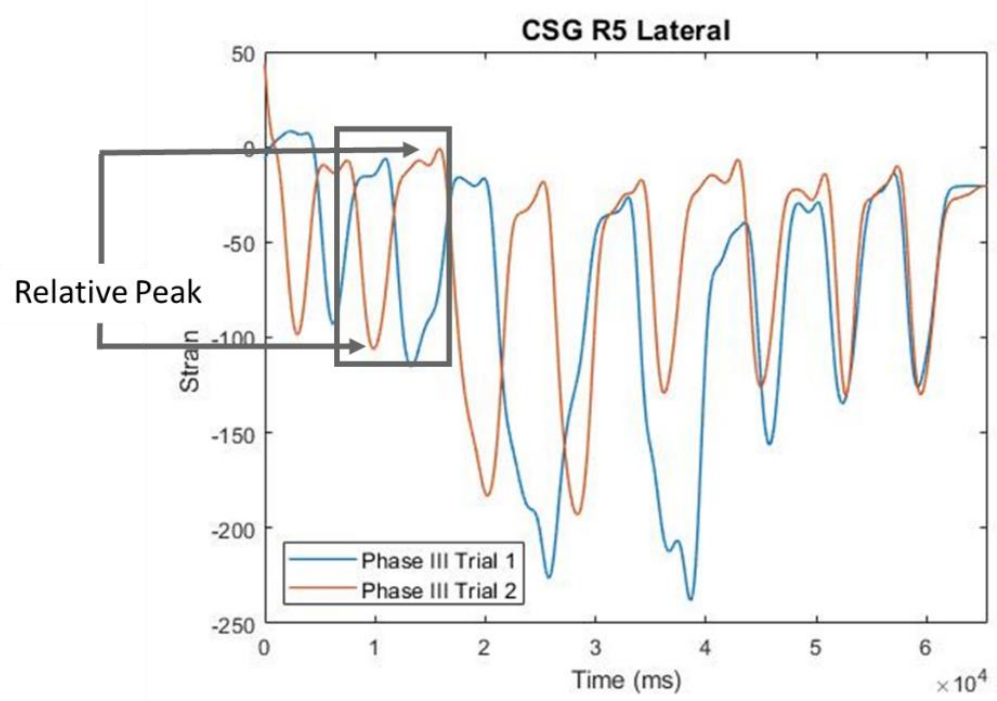

Figure 12. A visual representation of the relative peak measurement, which equates to maximum minus minimum strain over a single breath.

For each individual gage, a Mann-Whitney test was performed to compare the relative peak magnitudes. The shallow and deep breaths were compared separately, and each individual breath was treated as a single observation. At twenty-two of the forty-two individual strain gages, there was no significant difference between Phases II and III for shallow breaths ($p > 0.05$), and all forty-two individual gages did not show significant differences between Phases II and III for deep breaths ($p > 0.05$). The strain data from each rib level, including all three gages at both the left and right ribs, were combined such that observations at each location were all considered when computing statistics. A Mann-Whitney test was performed for each rib level (Table 4).

Table 4. A summary of the results of a Mann-Whitney tests comparing the cutaneous strain data from Phases II and III for each rib level, including all gages at bilateral positions. Values in bold are significant.

Rib Level	3	4	5	6	7	8	9	All
p-value (shallow)	**0.001**	0.075	0.232	**0.047**	0.567	0.183	0.389	0.164
p-value (deep)	0.216	0.869	0.343	0.803	0.439	0.379	0.641	0.355

The boxplots corresponding to each rib level are in Appendix A. The majority of the rib levels and gages, excluding level 3 during shallow ventilation, showed no significant difference in the cutaneous strain gage data from Phases II and III ($p > 0.05$). This confirmed there was no practical difference in rib loading between the PMHS with and without the chestband, thus validating the use of the chestband.

Validating Use of the Air Bladder

The cutaneous strain gage data from Phases III and IV were compared to validate the use of an air bladder as a surrogate for the PMHS lungs. The relative peak measurements from Phase III were compared to absolute peak measurements from Phase IV, because each of the six trials in Phase IV consisted of a single ventilation (Figure 13).

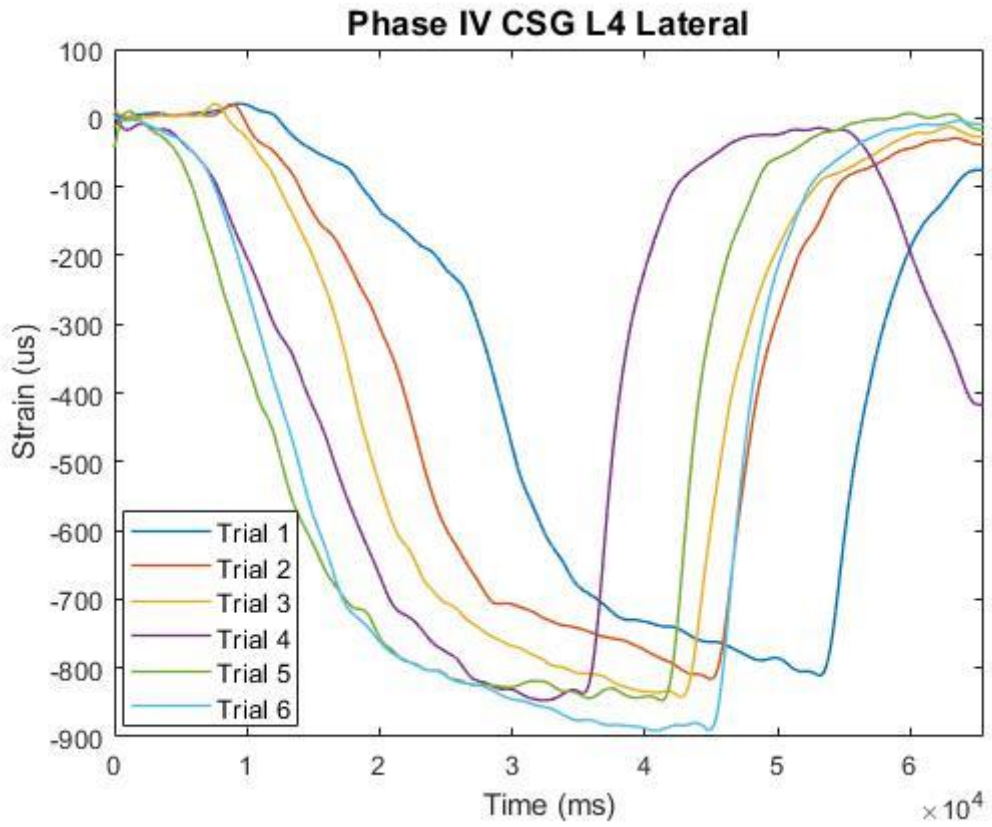

Figure 13. Time history plot of the lateral cutaneous strain gage at L4 during Phase IV.

A Mann-Whitney test was performed to compare the strain magnitudes. The relative peak of each breath was treated as a single observation, and all observations at each gage from Phase III were compared to all observations at the same gage from Phase IV. The majority of the cutaneous gages showed significant differences in strain magnitude between Phases III and IV ($p < 0.05$). This reflected the increased pressure expelled by the air pump, resulting in increased magnitudes of strain for Phase IV compared to Phase III (Figure 14).

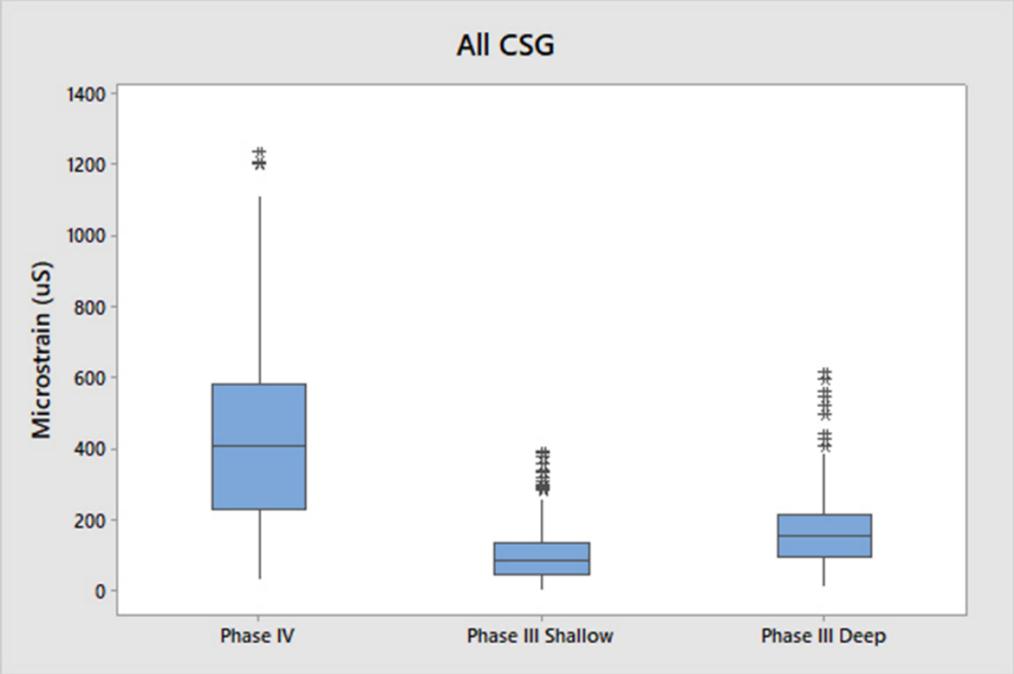

Figure 14. A boxplot of cutaneous strain magnitudes experienced at all gages for Phase III during both shallow and deep breaths and for Phase IV.

Based on the observed differences in magnitude between Phases III and IV, only the strain modes from Phase IV were used to draw conclusions. However, upon further review, there were inconsistencies in strain mode between Phase III and Phase IV for gages at the same location (Figure 15).

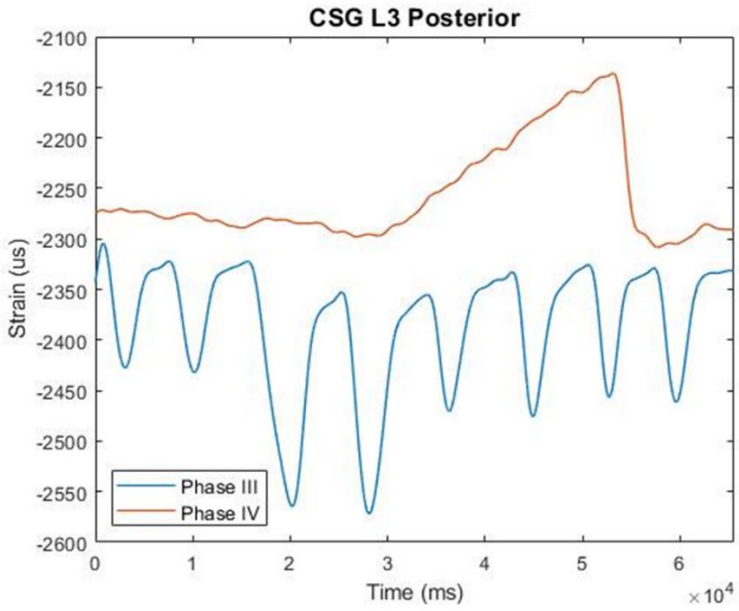

Figure 15. A time history plot from the cutaneous posterior gage on L3, which demonstrates tension in Phase IV (orange) and compression in Phase III (blue).

The strain modes for Phase IV were determined by the polarity of the single peak observed in each trial, and there were no inconsistencies between trials in the Phase IV at the same gage location. The strain modes for Phases II and III were determined similarly by the polarity of the peaks observed. For example, the blue plot of Phase III (Figure 15) is considered to be in tension because the deviation of the peaks from the momentary rest between breaths is in negative space. This is further confirmed with the presence of both shallow and deep breaths, where the exaggeration in shape and increased strain magnitude experienced during deep breaths is again directed in negative space. The polarity of each gage was qualitatively confirmed for all gages for Phases II through IV. To further investigate the inconsistencies in strain mode, the data acquisition systems and files were checked for errors in the data acquisition systems. When none were found, the inconsistencies were theorized to be artifacts of the morphological differences between the air bladder and PMHS lungs, among other inherent limitations of the system that are discussed further in the limitations section.

In light of the inconsistencies in strain mode between Phases III and IV at the same gage location, only gages consistent in strain mode for all of Phases II through IV were determined to be reliable and used in future analysis (Figure 16).

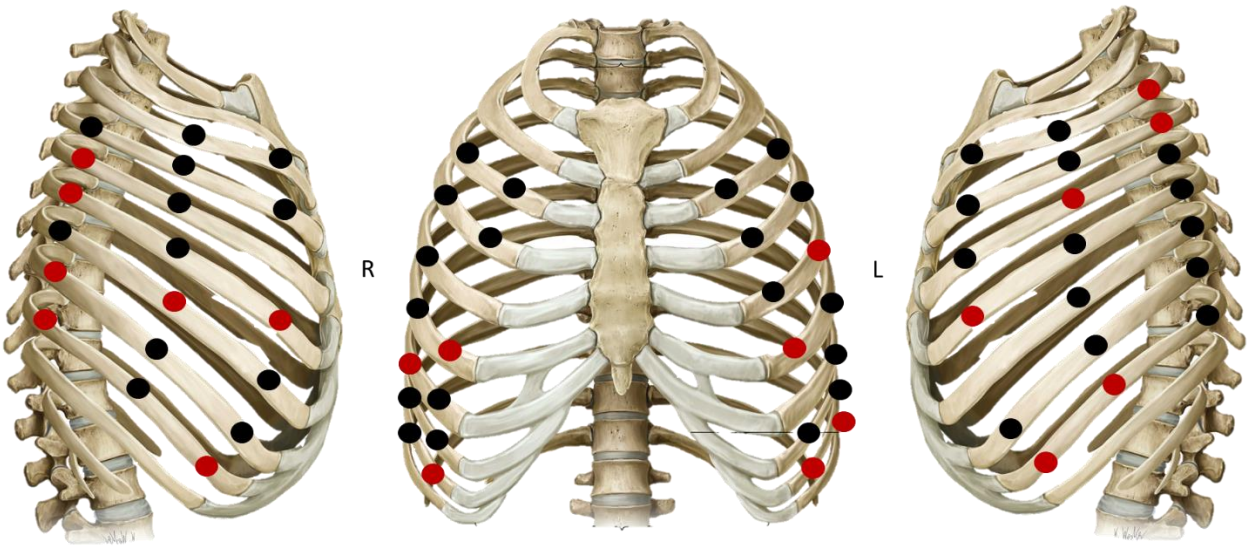

Figure 16. A map of all cutaneous strain gages applied to the thorax, with gages in black signifying they were consistent in modality from Phases II-IV and are thus considered valid.

Thirteen of the cutaneous gages were discarded as unreliable. For the remaining twenty-six gages, it was determined that comparisons of magnitude would rely on relative peak data from Phases II and III because they were shown to be similar to the *in vivo* magnitudes from Phase I. Comparisons of magnitude in Phase IV were drawn only within Phase IV. Comparisons of strain mode were consistent among all three Phases II through IV, thus comparisons would be drawn from all valid gages. For valid cutaneous strain gages, if there was a pleural gage present at the same location in Phase IV, the pleural gage was also considered valid.

Hypothesis I

The first hypothesis states that patterns of strain mode and magnitude would be consistent for all rib levels. All but one of the cutaneous strain gages on ribs three through five experienced the same strain mode, compression (Figure 17).

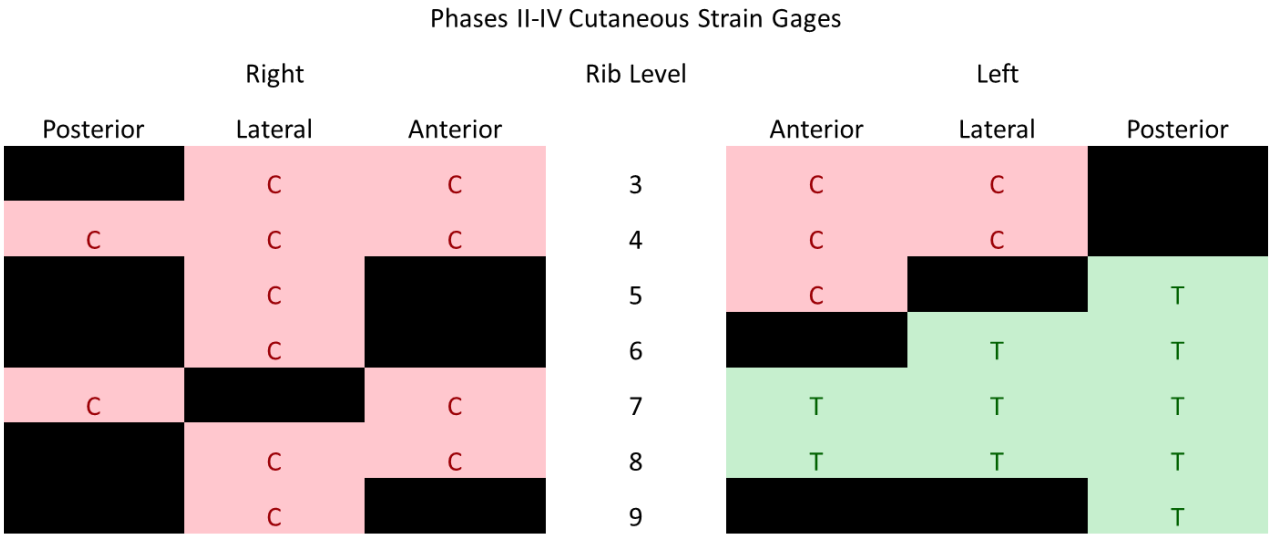

Figure 17. A representation of the strain modalities experienced at each gage, where boxes filled in black are invalid gages, boxes in green are in tension, and boxes in pink are in compression.

The same trend is not observed in the lower ribs, indicating the upper ribs demonstrate more synchronous behavior. This is in agreement with findings from past studies [13] and is anatomically logical, as the upper ribs demonstrate less variation in the angle of the costal cartilage. Furthermore, they are connected directly to the sternum, as opposed to the lower false or floating ribs that have a less robust anterior joint.

Additionally, while the external intercostal muscles recruited in ventilation to expand the thorax attach from the inferior border of one rib to the superior border of the next for every rib, the diaphragm originates near the inferior border of rib six and attaches to the costal cartilages of ribs seven through ten. While the central tendon of the diaphragm is at rib eight, it appears to exert a downward force when it contracts, affecting more of the lower ribs. Furthermore, the

right and left domes of the diaphragm are asymmetrical, as are the lungs, accounting for some of the bilateral variation in the lower ribs.

Hypothesis II

The second hypothesis states that patterns of strain mode and magnitude would be consistent between locations on the same rib. Only three ribs: R4, L7, and L8, had valid strain gages at all three locations. For this reason, it was difficult to draw conclusions corresponding to patterns across locations on a single rib; however, some noteworthy qualitative trends were observed. For the upper ribs, the highest magnitude of strain was experienced at the anterior gage for four of the five ribs measured (Figures 17, 18).

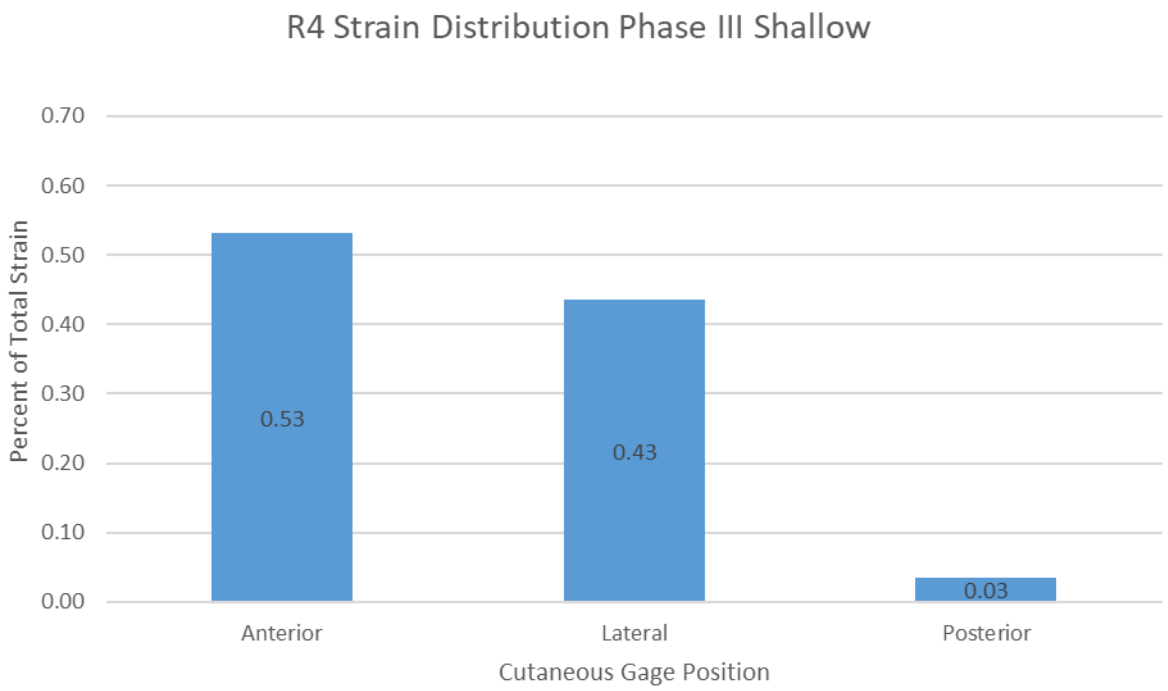

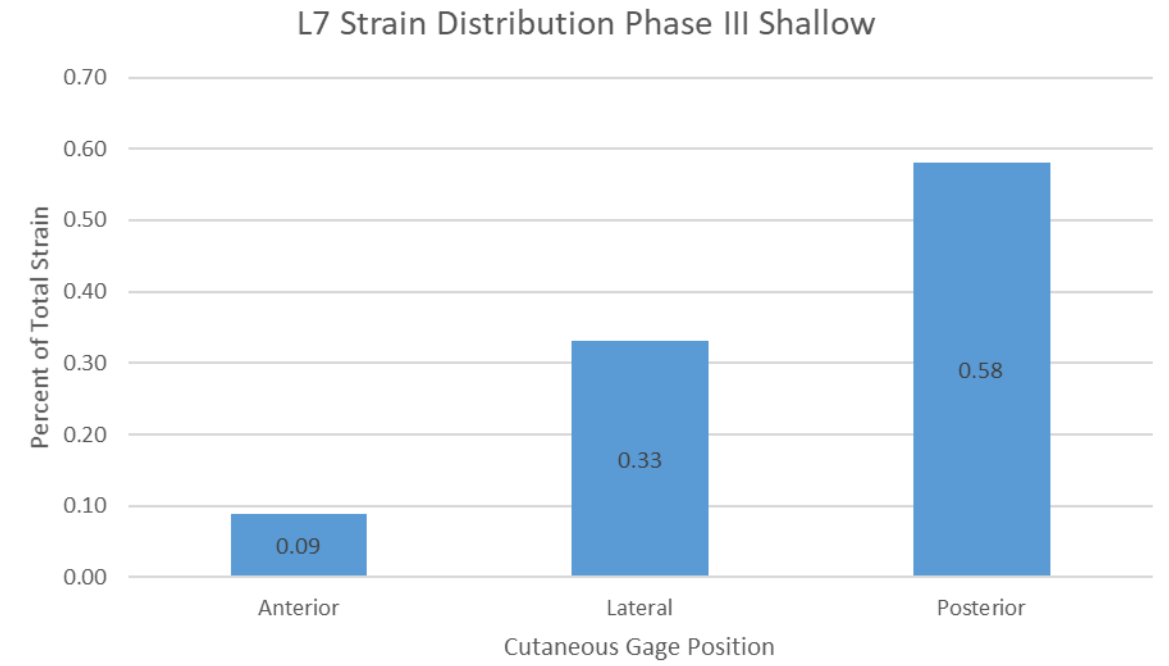

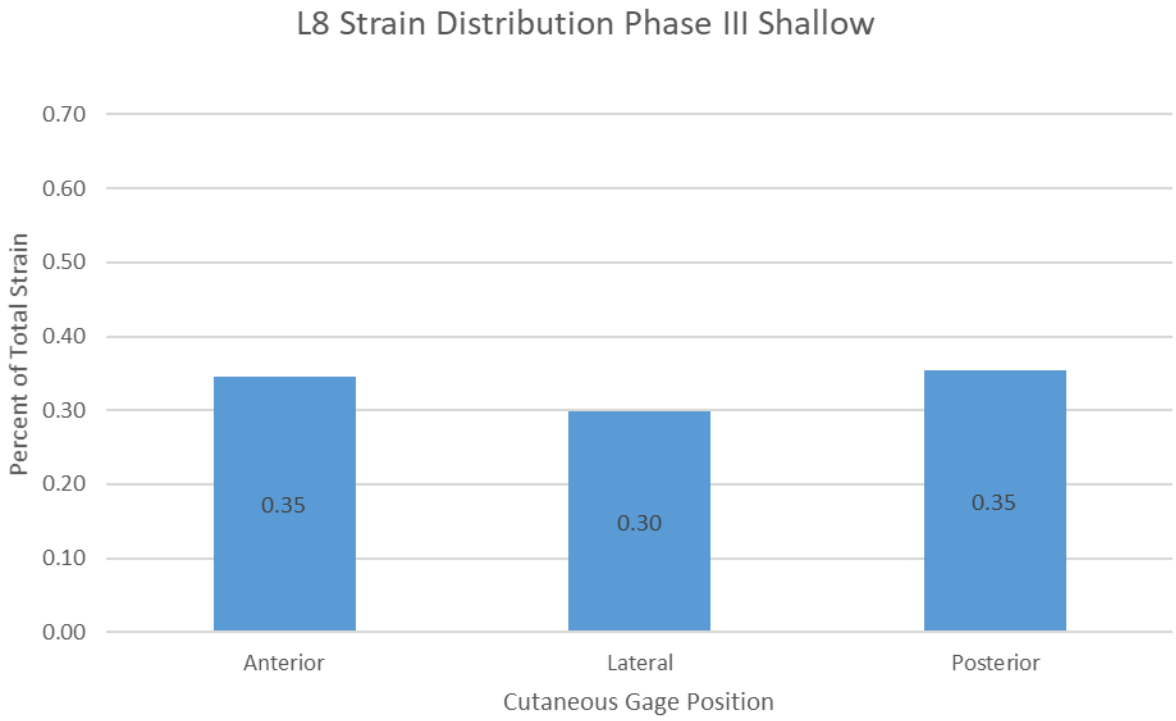

Figure 18. A plot of the strain distribution on the cutaneous gages of R4 (top), L7 (middle), and L8 (bottom) from Phase III shallow ventilations, calculated by percent of total strain experienced at each strain gage site.

The strain distribution plot for R4 (Figure 18) used the fraction of the median strain magnitude experienced at each individual site over the sum of the median strain experienced at all cutaneous gages on the rib to compute a percentage of the total strain that was present at each gage. The anterior gage at R4 experienced the greatest strain, and for the upper ribs with two or more gages, the anterior gage experienced the greatest magnitude of strain for the majority of them. The trend was more pronounced in the upper left ribs, visible by their increased vibrancy on the strain magnitude maps (Figure 19). The trend was also observed more consistently for R4 than R3, when comparing among Phases II and III.

Phase II Median CSG Shallow Strain Magnitude (uS)

Right			Rib Level	Left		
Posterior	Lateral	Anterior		Anterior	Lateral	Posterior
	132.80	97.87	3	182.73	35.38	
10.72	77.40	76.42	4	291.04	116.00	
	71.49		5	377.33		134.81
	22.77		6		59.26	111.44
58.75		234.63	7		24.82	126.92
	233.16	67.43	8	25.31	16.91	121.85
	121.98		9			41.23

Phase II Median CSG Deep Strain Magnitude (uS)

Right			Rib Level	Left		
Posterior	Lateral	Anterior		Anterior	Lateral	Posterior
	216.39	130.36	3	341.50	57.14	
26.31	141.86	85.49	4	532.23	210.41	
	125.06		5	840.92		349.63
	34.68		6		140.37	251.14
111.45		248.59	7		34.21	309.38
	369.74	64.07	8	52.64	53.46	321.10
	124.92		9			79.28

Phase III Median CSG Shallow Strain Magnitude (uS)

Right			Rib Level	Left		
Posterior	Lateral	Anterior		Anterior	Lateral	Posterior
	163	151	3	227	37	
8	105	129	4	357	149	
	112		5	283		98
	26		6		75	83
88		233	7	19	72	127
	155	41	8	100	87	103
	50		9			52

Phase III Median CSG Deep Strain Magnitude (uS)

Right			Rib Level	Left		
Posterior	Lateral	Anterior		Anterior	Lateral	Posterior
	244	201	3	360	54	
19	172	142	4	558	236	
	187		5	492		206
	70		6		162	191
189	66	222	7	21	145	262
	198	42	8	164	156	215
	71		9			111

Figure 19. Strain magnitude maps from Phases II and III with shallow (left) and deep (right) strain magnitudes. The magnitudes are highlighted by a gradient s.t. white is low magnitude and green is high, while black font is tension and red font is compression.

Interestingly, the strain distribution plots from L7 and L8 (Figure 18) indicate a completely different distribution of strain than the upper ribs. On L7, the highest strain was experienced at the posterior site, while at L8 the strain was relatively evenly distributed among all three locations. The lower rib levels, six through nine, qualitatively demonstrated higher strain magnitudes at the posterior locations in both Phases II and III (Figure 19). In contrary to the upper rib levels which experienced primarily compression, the lower rib levels also experienced primarily tension (Figure 19). The increased magnitude of strain experienced at the posterior gage location could be reasonably traced to anatomy, where the absence of a robust anterior attachment for the lower ribs aligns with the relatively low magnitudes of strain experienced at those locations. Likewise, the vertebral ends of the lower ribs are nearly fixed, which theoretically would lead to more strain at locations closed to that fixed point. This is especially true for the false or floating ribs, which could be likened to a cantilever beam with a single, fixed point of attachment, leading to a strain distribution much like L7 (Figure 18).

Hypothesis III

The final hypothesis states the cutaneous and pleural gages at the same location would be of opposite strain mode but similar magnitude. Due to difficulty in accessing the pleural cortex of the ribs, there were fewer pleural than cutaneous gages; however, twelve valid gage locations also had pleural gages. Of the twelve locations with both cutaneous and pleural gages, ten demonstrated opposing strain modes (Figure 20), such that if the cutaneous gage demonstrated tension, the pleural gage was in compression, and vice versa.

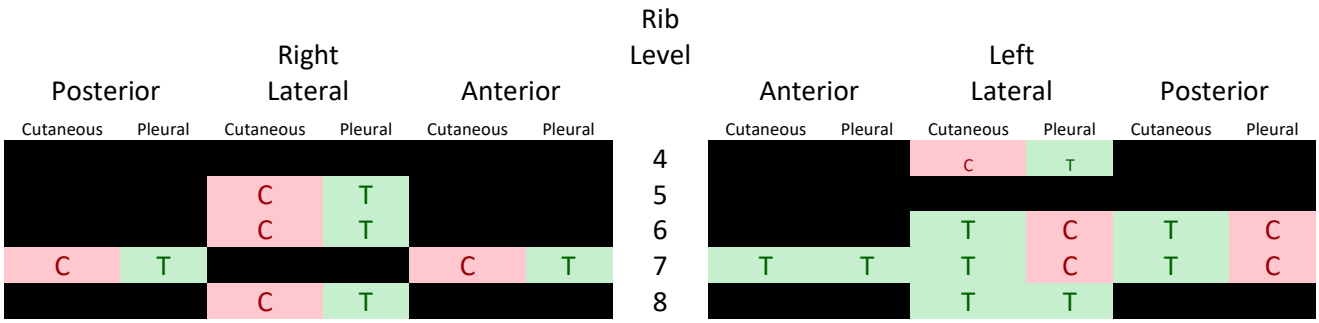

Figure 20. A map of the gage locations that experienced opposing cutaneous (left cell) and pleural (right cell) strain modes during Phase IV of testing. The pink cells indicate compression and the green cells indicate tension.

Furthermore, a Wilcoxon signed rank test was performed on the cutaneous and pleural strain magnitudes from Phase IV and the data were not significantly different ($p > 0.05$), indicating the strain magnitudes were similar (Figure 21).

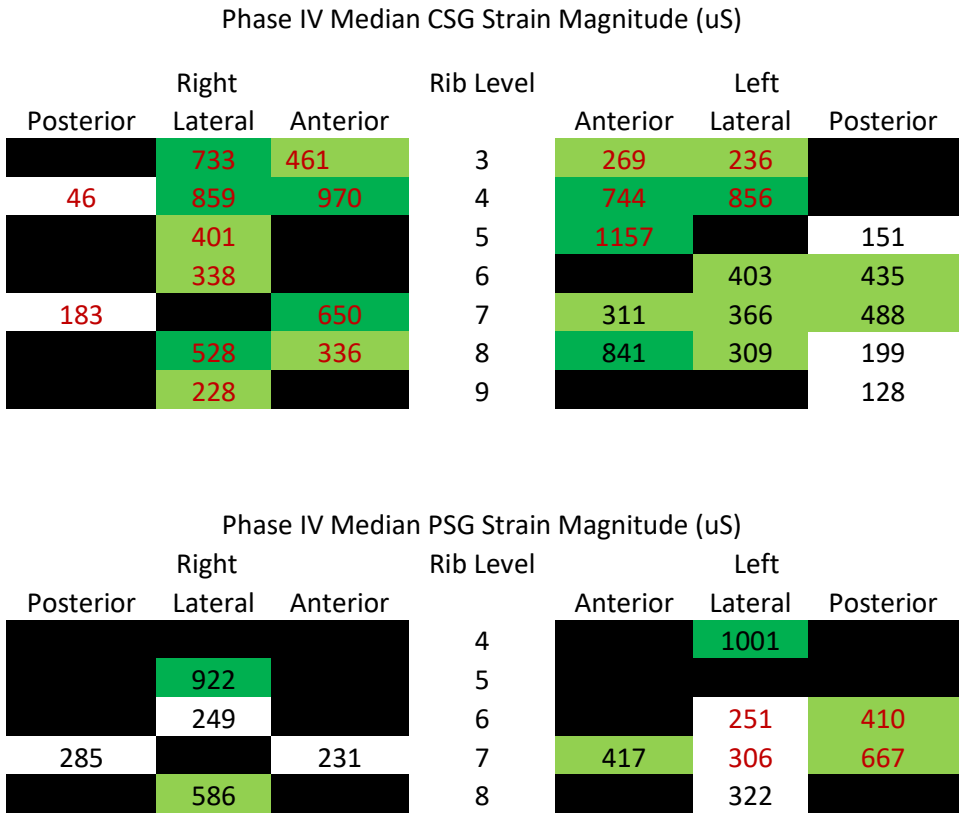

Figure 21. Maps of the cutaneous and pleural strain peak strain magnitudes from Phase IV.

The opposing strain modalities between cutaneous and pleural ribs is clear for the posterior site on L6 (Figure 22), where the cutaneous gage (in red) and pleural gage (in black) demonstrate time history plots of strain that are nearly perfect mirror images.

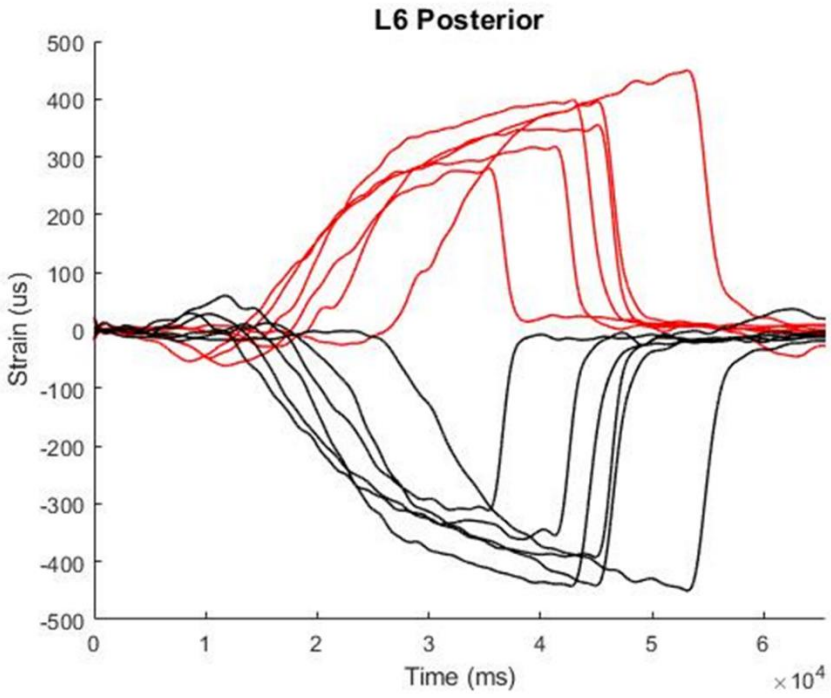

Figure 22. A time history plot of the cutaneous (red) and pleural (black) gage data from Phase IV, indicating strain coupling.

Force coupling is a more typical term associated with agonist and antagonist muscle groups, corresponding to muscles that simultaneously exert opposing forces, generating rotation but not translation. A similar idea was postulated in Hypothesis III, because rib cage expansion during ventilation relies on rotation at the anterior (sternal) and posterior (vertebral) rib joints. Visibly, the rib pivots outwards, in a process that appears rotation- and not translation-based. However, it is more difficult to make that generalization due to the unique morphology of a rib, leaving the center of mass likely somewhere outside the rib itself, due to the nature of a curved object. Thus, rotation about the center of mass would also generate some translation in the

curved object, accounting for the visible expansion of the ribs inwards and outwards during the process of ventilation.

Limitations

Major limitations of the study included inherent limitations of the PMHS system concerning a lack of muscle activation, especially in the diaphragm. The air bladder is an imperfect surrogate for the lungs, both spatially and because it does not fill uniformly. Thoracic wall compliance in the PMHS also differs from *in vivo* because the post-mortem tissue has different mechanical properties. Limitations of the instrumentation included the uniaxial nature of the strain gages and limits imposed by placing the gages at discrete locations on the ribs, thus allowing for quantification only at those locations. Finally, the pleural cavity was perforated on the right side of the thorax during instrumentation. While it was sealed, it still may have influenced results of the study.

Conclusions

Contributions

The present study contributed significantly to the existing knowledge of the internal loading environment experienced by ribs during ventilation. The PMHS system used in this study uniquely enabled quantifiable observation of strain experienced by the ribs due to the direct application of instrumentation to the ribs.

Additional Applications

The presented data correlate to a healthy model of ventilation, providing a baseline to which diseased models can be compared. Furthermore, the trends observed in the present study

can be used to verify trends in strain observed during lung pressurization prior to traumatic loading in biomechanical testing that relies on rib strain gages to determine thoracic injury. Finally, the trends observed can be used to inform and further investigate the morphological variation in ribs, especially relating to the presence of microcracks.

Future Work

Eventually, future work will include replicating Phase I of the study with multiple volunteers and Phases II-IV with multiple PMHSs. The current study can be built upon by creating functions to describe the rise and fall of strain magnitudes during ventilation at high pressure in Phase IV, and using those functions to generate expected strain during Phase III and using that to validate use of the air bladder in place of the lungs. More investigation into the timing of peak strain for different gage locations and different ribs during the same breath could also provide valuable insight. Furthermore, improvements in the strain gage application process will ensure more gages are valid and can be used to more fully address the hypotheses posed in the current study. It would also be interesting to delve into respiratory volumes and capacities of volunteer subjects and recapitulating those in a PMHS model.

Summary

This study verified rib strain patterns during ventilation can be determined in a PMHS model and identified patterns in strain modes and magnitudes across the thorax during ventilation. Future work will focus on utilizing these data to interpret morphological variation in human rib geometry and microstructure. The increased understanding of normal mechanical loading on ribs will contribute to understanding differential fracture risk.

References

1. Marder E. Variability, compensation, and modulation in neurons and circuits. Proc Natl Acad Sci 2011;108:15542–8.
2. Sanger TJ, Norgard EA, Pletscher LS, Bevilacqua M, Brooks VR, Sandell LJ, et al. Developmental and genetic origins of murine long bone length variation. J Exp Zool B Mol Dev Evol 2011;316B:146–61.
3. Olson EC, Miller RL. Morphological integration. Chicago, IL: University of Chicago Press; 1999.
4. Cheverud JM. Developmental integration and the evolution of pleiotropy. Am Zool 1996;36:44–50.
5. Waddington CH. Canalization of development and the inheritance of acquired characteristics. Nature 1942;14:563–5.
6. Wright S. Correlation and causation. J Agric Res 1921;20:557–85.
7. Jepsen KJ, Evans EJ, Negus CH, Gagnier JJ, Centi A, Erlich T, et al. Variation in tibial functionality and fracture susceptibility among healthy, young adults arises from the acquisition of biologically distinct sets of traits. J Bone Miner Res 2013;28:1290–300.
8. Al-Qadi MO. Clin Chest Med. 2018 Jun;39(2):361-375. doi: 10.1016/j.ccm.2018.01.010. Review.
9. Sharma G, Carter YM. Pectus Excavatum. [Updated 2019 Feb 22]. In: StatPearls [Internet]. Treasure Island (FL): StatPearls Publishing; 2019 Jan-.
10. Aaro, S. and Ohlund, C. (1984) Scoliosis and pulmonary function. Spine 9, 220-222.
11. Xu J-Q, Qiu P-L, Yu R-G, et al. Better short-term efficacy of treating severe flail

chest with internal fixation surgery compared with conservative treatments. Eur J Med Res. 2015;20:55.

12. Murach MM, Kang YS, Bolte JH 4th, Stark D, Ramachandra R, Agnew AM, Moorhouse K, Stammen J. Quantification of Skeletal and Soft Tissue Contributions to Thoracic Response in a Dynamic Frontal Loading Scenario. Stapp Car Crash J. 2018 Nov;62:193-269.
13. Beyer B, Feipel V, Sholukha V, Chèze L, Van Sint Jan S. In-vivo analysis of sternal angle, sternal and sternocostal kinematics in supine humans during breathing. J Biomech. 2017 Nov 7;64:32-40. doi: 10.1016/j.jbiomech.2017.08.026. Epub 2017 Sep 1.
14. Kenyon CM, Cala SJ, Yan S, Aliverti A, Scano G, Duranti R, Pedotti A, Macklem PT. Rib cage mechanics during quiet breathing and exercise in humans. J Appl Physiol (1985). 1997 Oct;83(4):1242-55.
15. Anatomy and Physiology by Rice University

Appendix A

Boxplots for Rib Level Comparison Between Phases II and III

The boxplots compare relative peak strain magnitude between Phases II and III. Each plot contains the relative peak strain magnitude observations from each breath, during each trial, at each gage location on the designated rib level.

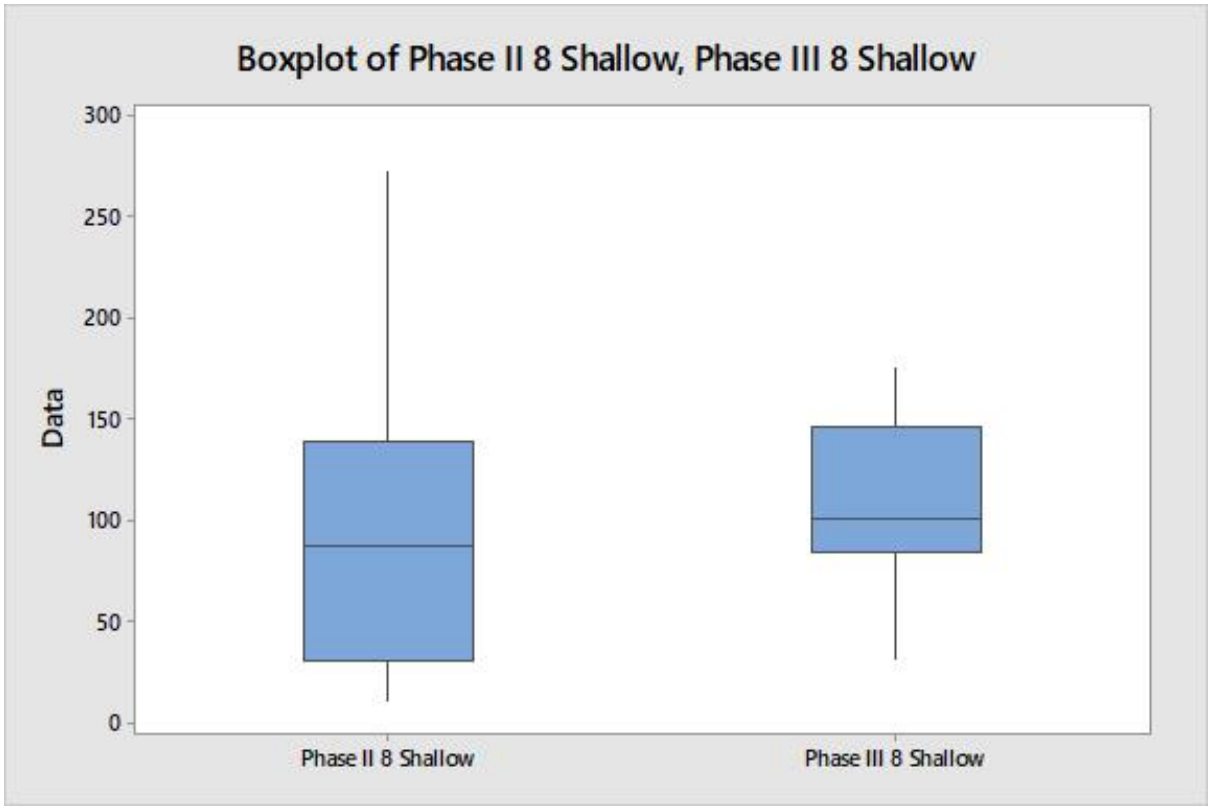
Boxplot of Phase II 8 Shallow, Phase III 8 Shallow
Data
300
250
200
150
100
50
0
Phase II 8 Shallow
Phase III 8 Shallow

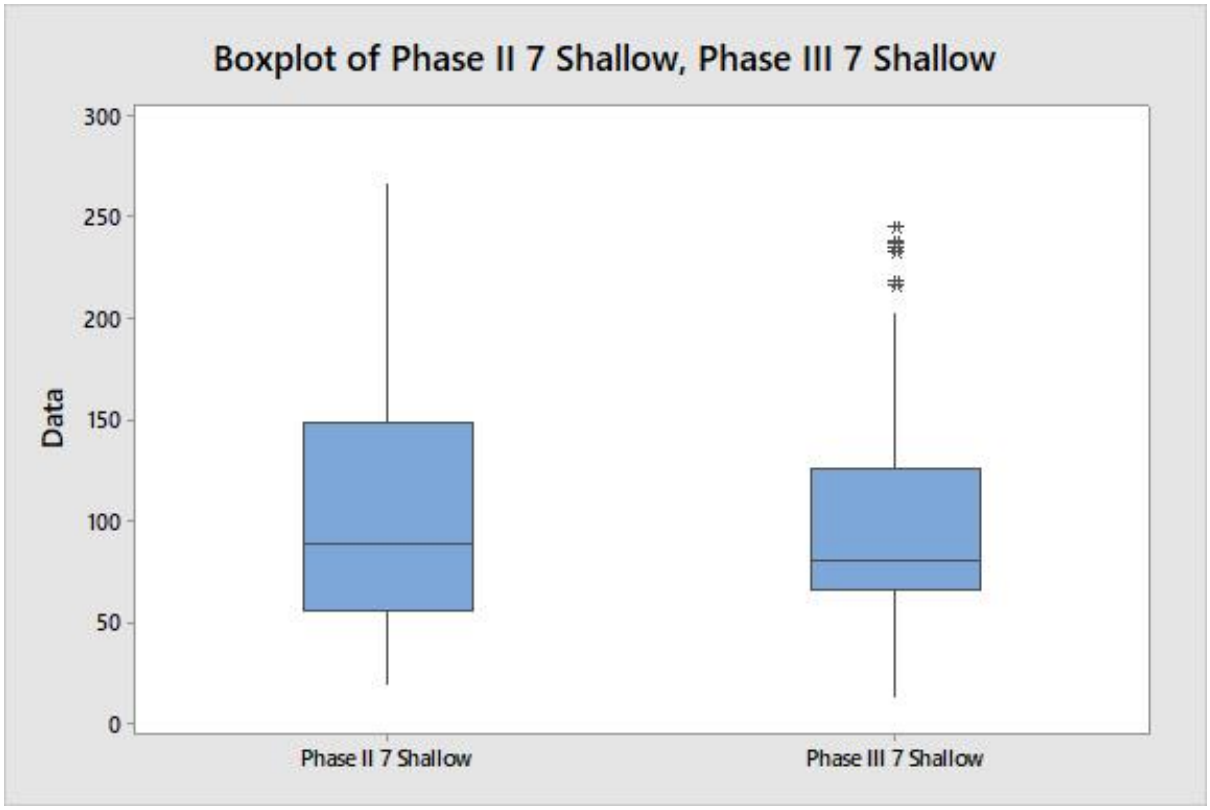
Boxplot of Phase II 7 Shallow, Phase III 7 Shallow
Data
300
250
200
150
100
50
0
Phase II 7 Shallow
Phase III 7 Shallow

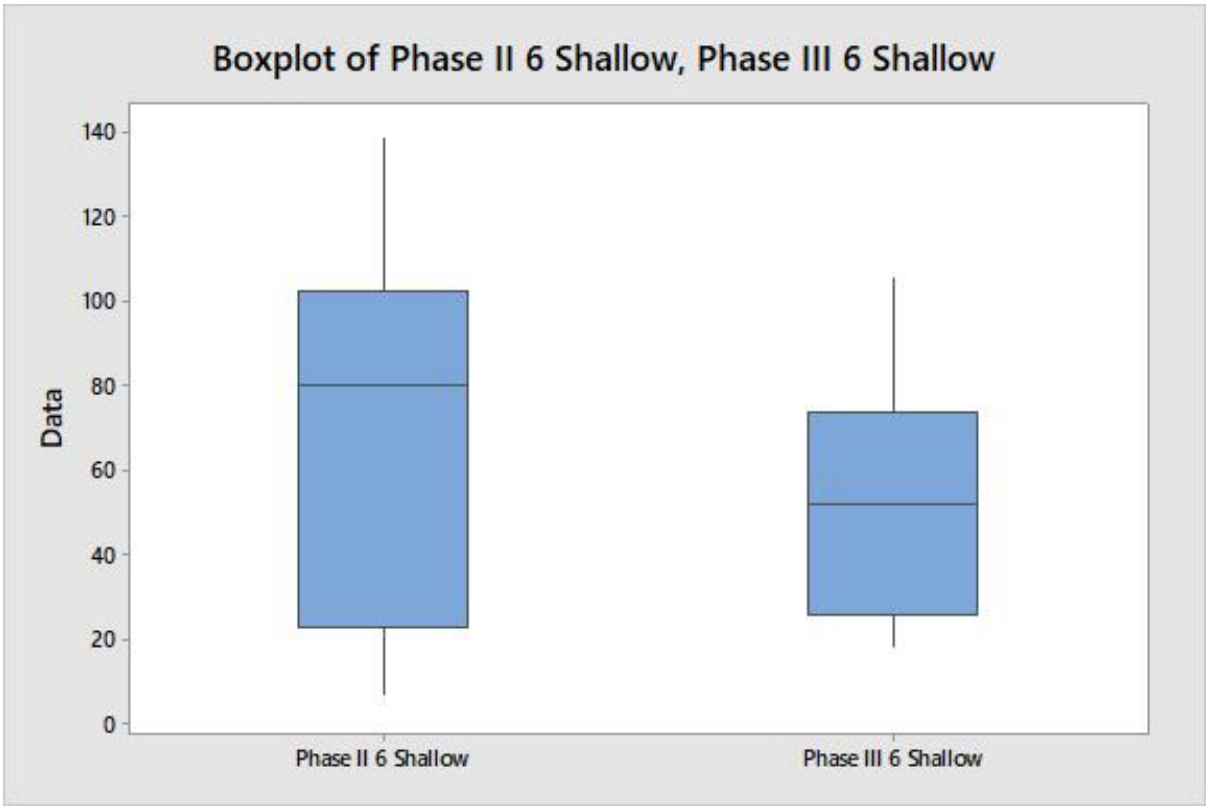
Boxplot of Phase II 6 Shallow, Phase III 6 Shallow
Data
140
120
100
80
60
40
20
0
Phase II 6 Shallow
Phase III 6 Shallow

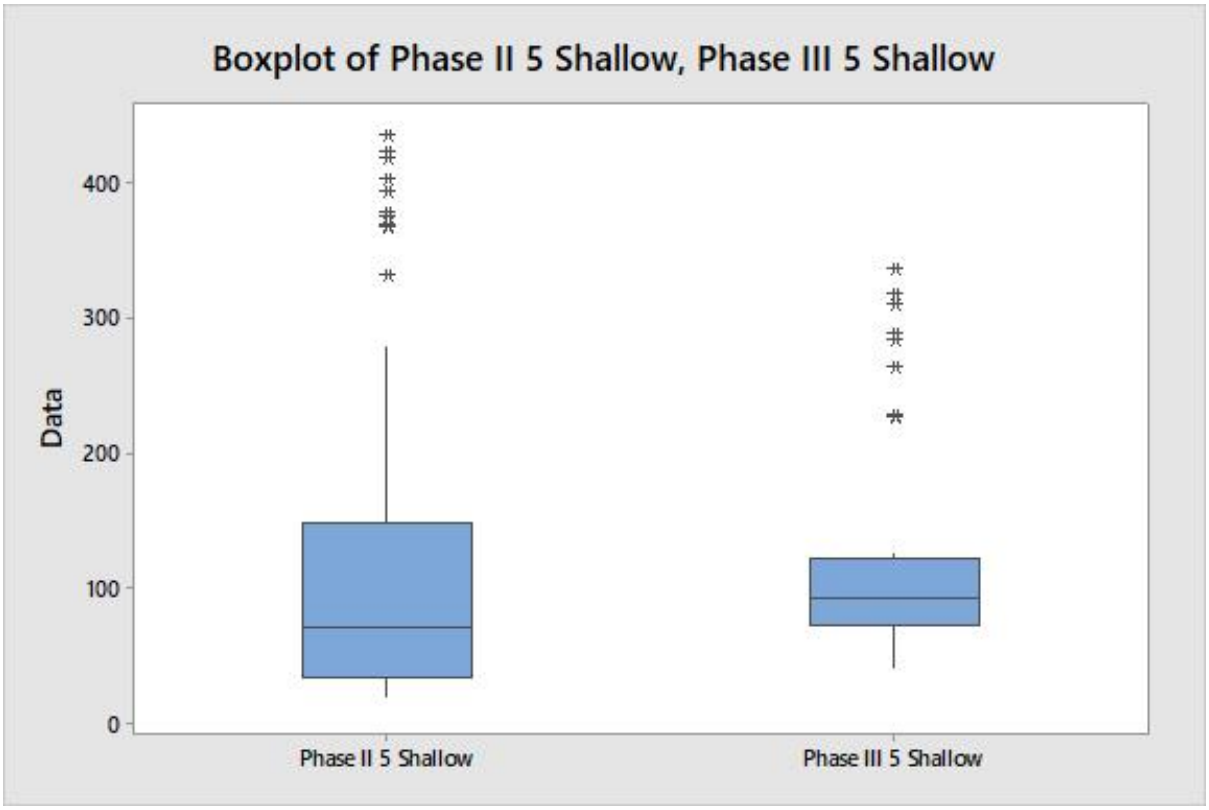
Boxplot of Phase II 5 Shallow, Phase III 5 Shallow
Data
400
300
200
100
0
Phase II 5 Shallow
Phase III 5 Shallow

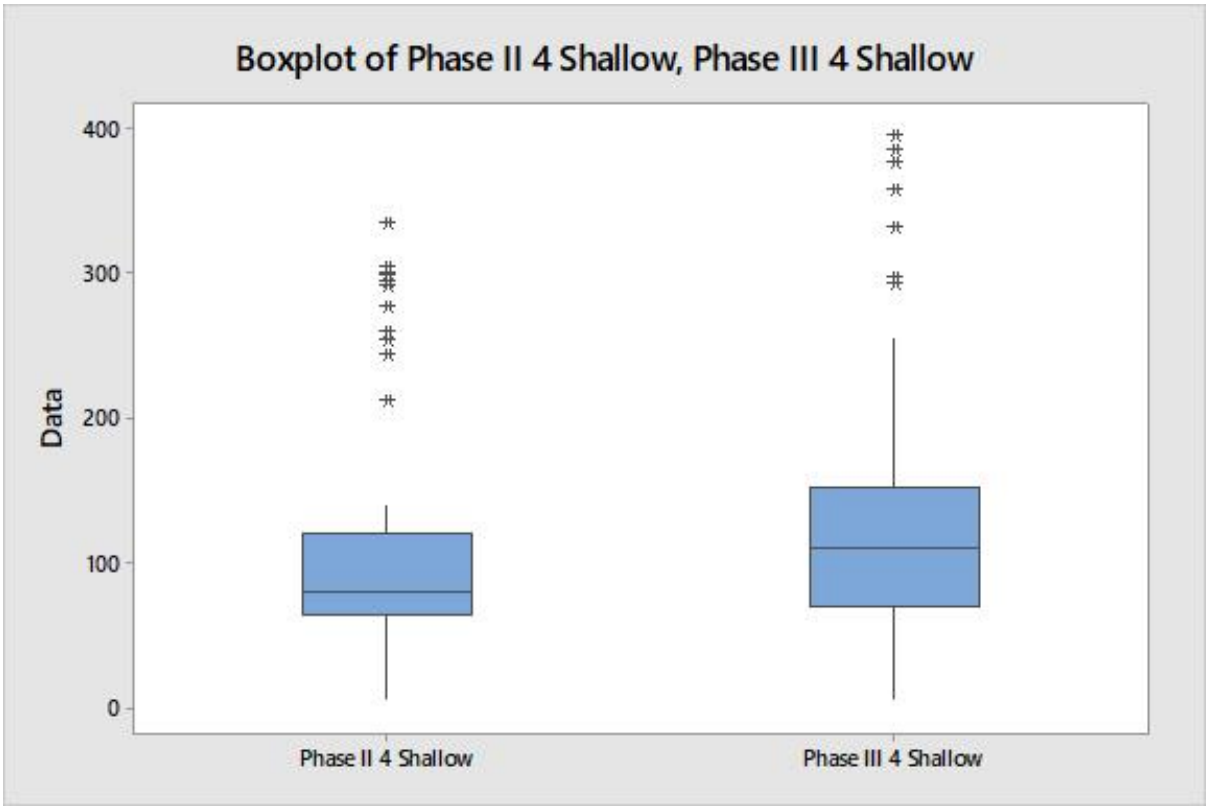
Boxplot of Phase II 4 Shallow, Phase III 4 Shallow
Data
400
300
200
100
0
Phase II 4 Shallow
Phase III 4 Shallow

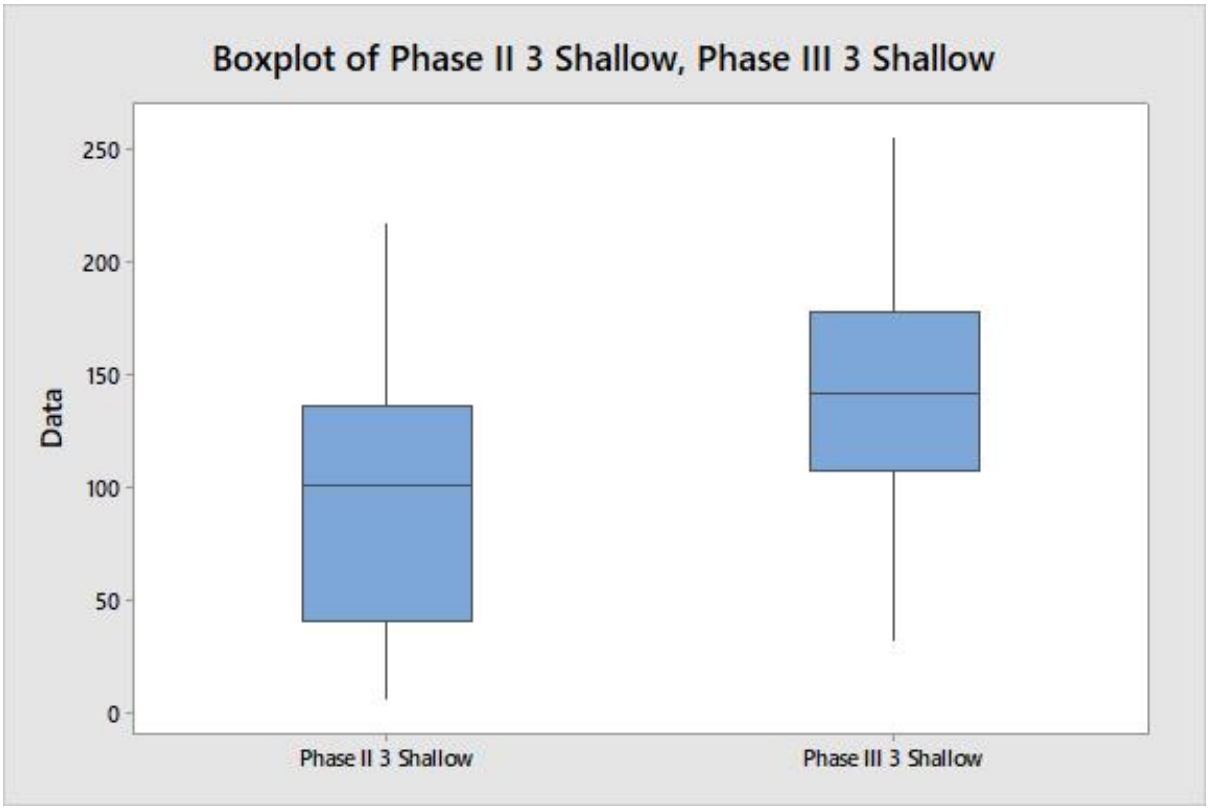
Boxplot of Phase II 3 Shallow, Phase III 3 Shallow
Data
250
200
150
100
50
0
Phase II 3 Shallow
Phase III 3 Shallow

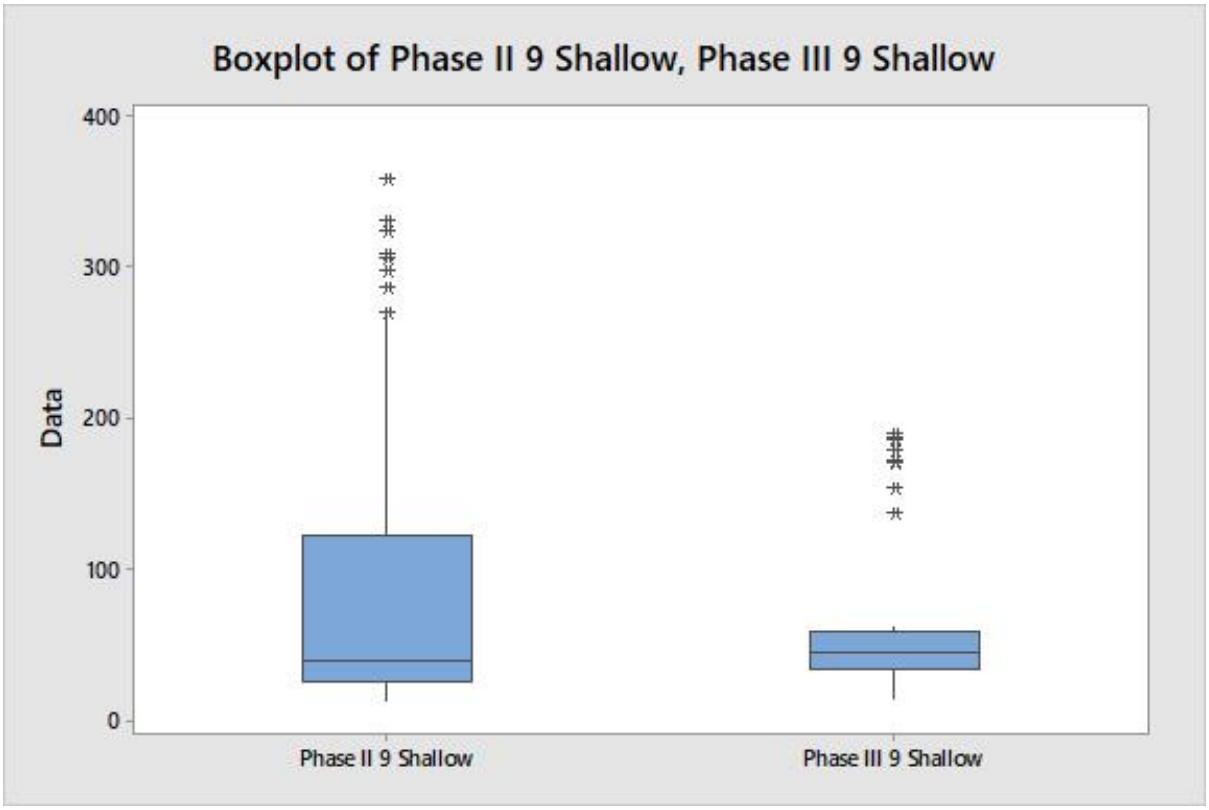
Boxplot of Phase II 9 Shallow, Phase III 9 Shallow
Data
400
300
200
100
0
Phase II 9 Shallow
Phase III 9 Shallow